PCCP

PAPER

View Article Online
View Journal | View Issue

Cite this: *Phys. Chem. Chem. Phys.*, 2025, **27**, 19445

Temperature dependence of reactions between aqueous manganese ions and water radiolysis products

Aliaksandra Lisouskaya, * Ian Talty, Brady Soenen and Nevis Dickson

Received 9th July 2025,
Accepted 8th August 2025

DOI: 10.1039/d5cp02625c

rsc.li/pccp

This study explores the temperature-dependent kinetics of reactions between aqueous Mn^{2+} ions and primary water radiolysis products, with emphasis on the transient behavior of short-lived manganese species. Rate constants for Mn^{2+} reactions with the hydrogen atom (H), hydroxyl radical ($^{\bullet}OH$), and superoxide ($O_2^{\bullet-}$) were determined across a pH range of 1–6 and a temperature range of 1–60 °C. All reactions followed Arrhenius behavior, indicating consistent thermal activation across redox pathways. The findings enhance our understanding of manganese redox chemistry in radiation-influenced systems, with implications for catalysis, energy conversion, and reactor chemistry.

Introduction

Manganese is a versatile transition metal with multiple accessible oxidation states (*e.g.*, Mn^{2+}, Mn^{3+}, Mn^{4+}, Mn^{7+}), making it a valuable component in a wide range of redox-driven applications. For example, manganese-based oxides and complexes are promising catalysts for environmentally important reactions like the oxygen evolution reaction in water electrolysis.[1–3]

Manganese chemistry is of interest in the context of nuclear energy and reactor coolant systems. In nuclear reactors, particularly light water reactors, manganese may enter aqueous phases as an impurity, alloy component, or additive for corrosion mitigation.[4] Radiolysis of water leads to the formation of highly reactive species such as hydrated electrons (e_{aq}^-), hydroxyl radicals ($^{\bullet}OH$), hydrogen atoms (H), and molecular species like H_2 and H_2O_2,[5] which can interact with dissolved manganese ions. These interactions may influence corrosion processes, redox equilibria, and metal ion transport in reactor coolant systems.[6,7] Understanding the fundamental kinetics of manganese ion reactions under radiolytic conditions is therefore critical to modeling and managing radiation chemistry in nuclear reactors.

Although manganese can exist in multiple oxidation states, this work focuses on Mn^{2+} because it is thermodynamically favored and remains soluble at near-neutral pH, while higher oxidation states (*e.g.*, Mn^{3+}, Mn^{4+}) tend to form insoluble oxides that precipitate out of solution. Furthermore, corrosion product analysis from irradiated structural alloys shows that Mn^{2+} is frequently observed.[4]

Notre Dame Radiation Laboratory, University of Notre Dame, Notre Dame, IN 46556, USA. E-mail: alisousk@nd.edu

Previous studies of Mn(II) reactions with water radiolysis products were conducted mainly at room temperature, with limited data on experimental conditions.[8–14] Additionally, transient absorption spectra were recorded only at select wavelengths. To fully understand the transient species formed and their kinetics—particularly across different temperatures—more detailed and comprehensive information is needed.

This work investigates the temperature dependence of reactions between aqueous Mn^{2+} ions and water radiolysis products, with particular focus on the formation and reactivity of short-lived manganese species using pulse radiolysis. Pulse radiolysis is a powerful time-resolved technique that enables the direct observation of short-lived reactive species formed during the radiolysis of water. In this method, a high-energy electron pulse initiates radiolysis by generating primary radical species.

Radiolysis in nuclear reactor coolant water occurs under complex conditions that differ significantly from those in pure water. The presence of dissolved salts, corrosion products, additives, and elevated temperatures and pressures, combined with intense radiation fields, greatly influences the chemical processes involved. To better understand these effects, we investigate the radiolysis of water containing dissolved metal ions across a range of temperatures. This approach simulates certain aspects of reactor conditions and provides insight into the behavior of highly reactive oxidizing and reducing species generated during radiolysis. The primary radiolysis products and their corresponding radiation-chemical yields (*G*-values) in pure,[5] deaerated water at room temperature are shown in eqn (1). These *G*-values represent the number of micromoles of a species produced per joule of energy absorbed from ionizing radiation (μmol J^{-1}). They are fundamental to

understanding the radiation chemistry of water, as they quantify the initial concentrations of reactive species. These *G*-values represent the escape yields from the spur—that is, the concentrations of radiolysis products that have survived early recombination reactions and become uniformly distributed in the bulk solution, typically by approximately 1 μs after the ionizing event.[15]

$$H_2O \rightsquigarrow 0.29e_{aq}^-,\ 0.29^{\bullet}OH,\ 0.062H,\ 0.046H_2,\ 0.073H_2O_2,\ 0.29H_{aq}^+ \quad (1)$$

These radiolysis products rapidly undergo secondary reactions, and the presence of metal ions in solution can significantly influence their reaction pathways and kinetics. In this study, we determine the rate constants for the reactions of aqueous Mn(II) ions with the reducing e_{aq}^-, H and the oxidizing $^{\bullet}OH$ (eqn (1)). To better simulate the chemical environment of nuclear reactor coolant water and energy conversion systems, we also examined reactions in oxygenated solutions. In the presence of dissolved oxygen, hydrated electrons rapidly react to form superoxide ($O_2^{\bullet -}$), introducing an additional reactive species that can further influence manganese redox chemistry.

The transient species formed from the reaction of water radiolysis products with metal ions are monitored in real time using spectroscopic detection, enabling precise determination of their kinetics. Temperature-dependent analysis of these reactions provides insight into activation parameters and underlying mechanistic pathways, which are relevant to radiation-driven processes in reactor chemistry.

Our findings deepen understanding of manganese redox chemistry in irradiated aqueous environments and offer insights applicable not only to nuclear reactor chemistry but also to catalysis and energy conversion systems where similar redox processes occur.

Experimental

Materials

Solutions of $MnSO_4{\cdot}4H_2O$ (Thermo Scientific, ≥99%), $MnCl_2{\cdot}4H_2O$ (Sigma-Aldrich, ≥98%) and $Mn(ClO_4)_2$ hydrate (Sigma-Aldrich, ≥99%) were prepared at concentrations from 0.1 to 10 mM. Prior to use, the solutions were saturated with ultrahigh-purity Ar, N_2O or O_2 gases (Airgas), which were used throughout the experiments. Methanol (≥99.5%), sodium formate (99.998%), and *tert*-butanol (anhydrous, ≥99.5%) were purchased from Sigma-Aldrich. All solutions were prepared using ultrapure water (18 MΩ cm resistivity, <10ppb TOC) from a Serv-A-Pure Co. cartridge system. All other chemicals were also obtained from Sigma-Aldrich and used without further purification.

Pulse radiolysis

Pulse radiolysis was carried out using an 8 MeV Linear Accelerator (LINAC) at the Notre Dame Radiation Laboratory, University of Notre Dame. The detection system consisted of a xenon arc lamp light source and a multichannel detection system capable of recording two-dimensional transient absorption *vs* time traces over a full spectrum as described earlier.[16] The experiments used a 1.0 cm pathlength quartz optical cell with a single-pass flow-through setup to prevent product build-up. For temperature-dependence studies, gas-saturated solutions were placed in the quartz cell and cooled to 1 °C or heated to 65 °C at atmospheric pressure using a TLC 50/E thermoelectric-temperature controlled 4-window cuvette holder (Quantum Northwest, Inc.). For radiation dosimetry, 10 mM KSCN solutions saturated with N_2O were employed; the value $G \times \varepsilon$ of $(SCN)_2^{\bullet -}$ at 475 nm was taken as $(5.3 \pm 0.10) \times 10^{-4}$ m^2 J^{-1}.[17]

All measurements were carried out using radiation doses ranging from 6 to 50 Gy and at least four different salt concentrations. Each experiment was repeated a minimum of three times to ensure reproducibility.

Data fitting was carried out using the IGOR Pro software package (WaveMetrics, Inc.). Kinetic simulations (global fitting) were conducted by integrating the relevant partial differential equations. These kinetic models were then used to extract the rate constants of the reactions. Corrections were applied to account for changes in the absorbed radiation dose resulting from the decrease in water density at elevated temperatures. Additionally, the rate constants were corrected for ionic strength effects using the Debye–Brønsted equation.[16,18] All reported rate constants are presented at zero ionic strength.

Results and discussion

Reactivity of Mn^{2+} with the hydrated electron

The reaction between Mn^{2+} and e_{aq}^- (eqn (2)) was studied in an Ar-saturated solution, where manganese(II) exists as the hexa-aquo ion coordinated by six water molecules. Saturating the solution with argon removes dissolved oxygen and other reactive gases from the air, preventing unwanted side reactions with radiolysis products and ensuring that observed kinetics reflect only the intended Mn^{2+} reactions. To obtain precise data, manganese(II) salts with different anions were examined. Electron decay was analyzed in an Ar-saturated system both with and without methanol, which acts as a hydroxyl radical scavenger to prevent potential interactions between Mn^{2+} and $^{\bullet}OH$.

$$Mn^{2+} + e_{aq}^- \rightarrow Mn^+ \quad (2)$$

Fig. S1 (SI) presents kinetic traces depicting the decay of the e_{aq}^- absorbance at 717 nm following a 10 ns, 24.8 Gy pulse at 25 °C in the presence of Mn(II) salt at pH 5. The dashed black lines correspond to fitted curves using single exponential decays. The obtained pseudo-first-order rate constants (k') were plotted against $MnSO_4$ concentration to determine the second-order rate constants (Fig. S1, inserts).

The rate constant determined in our study using two different salts at pH 5 was 2×10^8 M^{-1} s^{-1} at 25 °C, as fitted by an exponential decay. This value is slightly higher than those reported in the literature, as shown in Table 1.[8–10] However, when using a global fitting approach (see Experimental section), that includes the competing reaction of protons with e_{aq}^-

Table 1 Rate constants of the reactions of Mn^{2+} with water radiolysis species at room temperature

Reaction	λ, nm	Rate constant, $k \times 10^7$ M^{-1} s^{-1}
$Mn^{2+} + e_{aq}^- \rightarrow Mn^+$	720	2.4 (this work);[a] 5.5;[8] 3.8;[9] 0.9 (0.5 M)[10]
$Mn^{2+} + H \rightarrow Mn^+ + H^+$	290	10 (this work);[a] 66 (0.01 M in H_2SO_4);[11] 20[12]
	346	13 (this work)[a]
$Mn^{2+} + {}^{\bullet}OH \rightarrow Mn^{3+} + OH^-$	290	1.0 (pH 5),[a] 2.5 (pH 3; this work);[a] 2.6 (pH 9, 260 nm);[13] 3.4 (pH 6.7, 260 nm);[10] 2.0 (pH 0–6)[12]
	346	6.2 (pH 3; this work)[a]
	480	1.3 (pH 5 and 3; this work)[a]
$Mn^{2+} + O_2^{\bullet -} \rightarrow [Mn{-}O_2]^+$	278	4.3 (pH 5; this work);[a] 5 (0.1 M KH_2PO_4, 5 mM HCOOH);[14] 11 (pH 6.7, 10 mM HCOOH);[10] 4 (pH 5, H_2SO_4);[12] 0.01 (pH 10)[24]
	425	3.5 (pH 5; this work)[a]

[a] The rate constants measured in this work were corrected to account for the ionic strength of the solution. Quoted errors are the standard errors of the linear least squares fit.

(eqn (3)), the determined rate constant decreases to 2.4×10^7 M^{-1} s^{-1}. These rate constants were corrected for ionic strength. Notably, the pH of the solution was not specified in previous studies, nor was there a correction for ionic strength in some of those papers.

$$H^+ + e_{aq}^- \rightarrow H,\ k = 2.1 \times 10^{10}\ M^{-1}\ s^{-1} \text{ at } 25\ ^\circ C \qquad (3)$$

In the experiments with 10 mM Mn(II), we observed the formation of monovalent Mn(I) transient species, which exhibit absorption in the UV region. Fig. 1A shows the transient absorption spectra (ε, $M^{-1}cm^{-1}$) recorded after 15-ns pulse radiolysis in Ar-saturated solutions containing 10 mM $MnSO_4$ and $MnCl_2$ (29 and 45 Gy) at pH 5 and room temperature. The intensity of the signal is weak. Importantly, no significant differences in the transient spectra or rate constants were observed between different counterions, indicating that the nature of the accompanying anion does not appreciably affect the formation or stability of Mn(I) species under these conditions.

The formation kinetics of Mn(I) at 290 nm, compared to 360 nm and 532 nm, over a timescale of 100 microseconds following the electron pulse, are shown in Fig. 1 (insert). As seen in the figure, the formation of the monovalent species is clearly evident at 290 nm and 360 nm; however, the formed Mn(I) species remain stable up to 400 microseconds under the studied conditions.

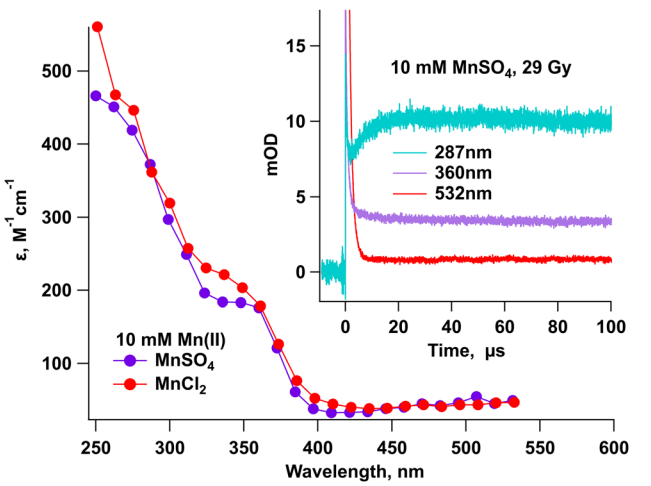

Fig. 1 Transient absorption spectra (ε) observed after 15-ns pulse radiolysis in Ar-saturated solutions with 10 mM $MnSO_4$ and $MnCl_2$ (29 Gy) at pH 5 at room temperature. (Insert) Kinetics of Mn^+_{aq} at 287 nm, 360 nm and decay kinetics of hydrated electron at 532 nm formed on 15 ns-pulse radiolysis (29 Gy) of 10 mM $MnSO_4$ solutions saturated with Ar.

By applying a global fit that incorporates the full set of water radiolysis reactions (Table S1, SI) along with reactions involving metal ions, the decay of the e_{aq}^- at 532 nm and the formation of Mn^+ at 287 nm were analyzed (Fig. S2, SI). This approach allowed us to estimate the reaction rate for eqn (2) and determine the extinction coefficient of Mn^+. The extinction coefficient $\varepsilon_{287\ nm}$ at room temperature was found to be 372 ± 27 $M^{-1}cm^{-1}$ formed from sulfate and chloride salts at pH 5.0. These numbers were derived based on $G(e_{aq}^-)$ (eqn (1)), adjusted to account for the concentration-dependent effects on spur decay kinetics and scavenging efficiency. Minor competing scavenging of e_{aq}^- by protons was also corrected by fitting the change in optical absorbance using a system of coupled ordinary differential equations that represent the chemical reactions taking place (Fig. S2 and Table S1 in SI). There are no published data on the extinction coefficient of Mn^+ in water.

Under the studied conditions, monovalent Mn ions remain stable on the millisecond timescale, making it difficult to measure their decay kinetics. Reducing the salt concentration could help capture this decay kinetics, but it would also weaken the signal. According to the literature,[19] hydrated monovalent manganese ions has a coordination number of 4 and exists in a septet state. In this study, the authors investigated $Mn^+(H_2O)_n$, using infrared multiple photon dissociation spectroscopy (IRMPD) and FT-ICR mass spectrometry.[19] They found that the non-inserted isomer of $Mn^+(H_2O)_4$ forms directly in the laser vaporization ion source, while the inserted isomer, $HMnOH^+(H_2O)_3$, is selectively produced by gently removing water molecules from larger clusters. Based on these data, we can assume that in an aqueous solution, Mn^+ exists in a septet state ($4s^13d^5$) and is coordinated by four water molecules in its first solvation shell.

We probed the influence of the pH on the absorption spectrum of the monovalent manganese ion formed during pulse radiolysis of 10 mM $MnSO_4$ solutions saturated with Ar (Fig. 2A). We prepared Mn(II) solutions at pH 1.6–3.2 by adding perchloric acid, and at pH 5.9 by adding sodium hydroxide.

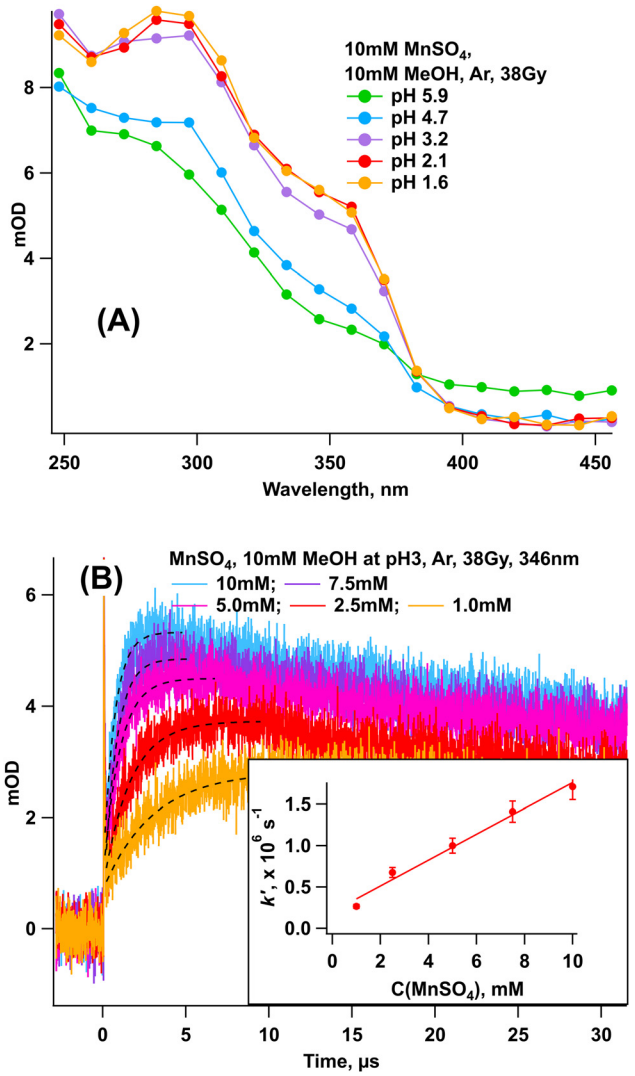

Fig. 2 Transient absorption spectra (A) and kinetics at 346 nm (B) observed 5 μs after 12-ns pulse radiolysis (38 Gy) in Ar-saturated $MnSO_4$ solutions at different pH at room temperature. ((B), insert) Pseudo-first-order rate constants (k') plotted against the $MnSO_4$ concentration to obtain second-order rate constants.

In an acidic solution, e_{aq}^- compete with added protons in a reaction (eqn (3)) with a rate constant of 2×10^{10} M^{-1} s^{-1} at room temperature.

As a result, we expect a lower intensity signal for Mn^+ under acidic conditions compared to neutral pH, since electrons are scavenged in the competing reaction (eqn (3)).

In solutions of $MnSO_4$ and $MnCl_2$ at pH 3, we observed transients originating from anions—such as sulfate radical anion ($SO_4^{\bullet -}$) at 470 nm (ref. 20) and dichloride radical anion ($Cl_2^{\bullet -}$) at 360 nm (Fig. S3 in SI).[21] The observed transients are generated through reactions with $^\bullet$OH originating from HSO_4^-, as shown in eqn (4), and with Cl^-, which undergoes a three-step reaction pathway described in eqn (5)–(7).

$$^\bullet OH + HSO_4^- (H_2SO_4) \rightarrow SO_4^{\bullet -} (HSO_4^\bullet) + H_2O(H_3O^+), \quad k = 4.7 \times 10^5 (1.4 \times 10^7)\ M^{-1}\ s^{-1} \text{ at } 25\ ^\circ C \tag{4}$$

$$^\bullet OH + Cl^- \rightarrow ClOH^{\bullet -}, \quad k = 3.0 \times 10^9\ M^{-1}\ s^{-1} \text{ at } 25\ ^\circ C \tag{5}$$

$$ClOH^{\bullet -} + H^+ \rightarrow Cl^\bullet + H_2O, \quad k = 2.1 \times 10^{10}\ M^{-1}\ s^{-1} \text{ at } 25\ ^\circ C \tag{6}$$

$$Cl^- + Cl^\bullet \rightarrow Cl_2^{\bullet -}, \quad k = 8.0 \times 10^9\ M^{-1}\ s^{-1} \text{ at } 25\ ^\circ C \tag{7}$$

In contrast, when 10 mM methanol was used to scavenge $^\bullet$OH, these transient signals were no longer detected in the corresponding spectral regions. Under these conditions, $^\bullet$OH are expected to be scavenged by methanol (eqn (8)), since methanol reacts with $^\bullet$OH much faster than anions do.

Alternatively, H atoms are unlikely to be scavenged by methanol (eqn (9)), because their reaction with methanol is much slower than their reaction with Mn(II) at the concentrations used in the experiments.

$$^\bullet OH + CH_3OH \rightarrow {}^\bullet CH_2OH + H_2O, \quad k = 9 \times 10^8\ M^{-1}\ s^{-1} \text{ at } 25\ ^\circ C \tag{8}$$

$$H + CH_3OH \rightarrow {}^\bullet CH_2OH + H_2, \quad k = 3 \times 10^6\ M^{-1}\ s^{-1} \text{ at } 25\ ^\circ C \tag{9}$$

In acidic $MnSO_4$ solution, we observed a more intense signal at 287 nm and an additional peak between 330 and 360 nm (Fig. 2A and B). However, the formation rates of this peak could not be detected at pH 5, as shown in Fig. 1(insert). The formation of this transient can be explained by the reduction of Mn^{2+} with H atoms formed in eqn (3), as shown in eqn (10) and as previously proposed.[11]

$$Mn^{2+} + H \rightarrow Mn^+ + H^+ \tag{10}$$

The rate constant for the formation of the transient at room temperature at 346 nm at pH 3 is 1.3×10^8 M^{-1} s^{-1} (Fig. 2B), while at 287 nm it is 1.0×10^8 M^{-1} s^{-1}. Dainton *et al.* reported a rate constant of 6.6×10^8 M^{-1} s^{-1} at room temperature for the reaction between Mn(II) and H atoms, based on changes in transient optical absorption at 290 nm in acidic $MnSO_4$ solutions.[11] These values were not corrected for ionic strength, and their experiments were conducted in $0.5–5 \times 10^{-2}$ M $MnSO_4$ solutions. Jacobsen *et al.* observed a similar transient spectrum in the reaction described by eqn (10), with absorption peaks at 290 nm and 340 nm and a rate constant of 2×10^8 M^{-1} s^{-1} at 25 °C.[12] This value is closer to the rate constant obtained in our study.

To study the temperature dependence of the reaction kinetics, we performed additional experiments at pH 3 in argon-saturated $MnSO_4$ solutions. We measured the rate constants of the transients formed at 287 nm and 346 nm over a temperature range from 1 °C to 60 °C. However, experimental limitations prevented us from extending the temperature range up to 300 °C because we observed rapid precipitation starting at 60 °C, making transient absorption measurements under these conditions infeasible. This behavior is discussed in more detail in the following section. The rate constants at different temperatures are provided in Table S2 of the SI. Fig. 3 shows the

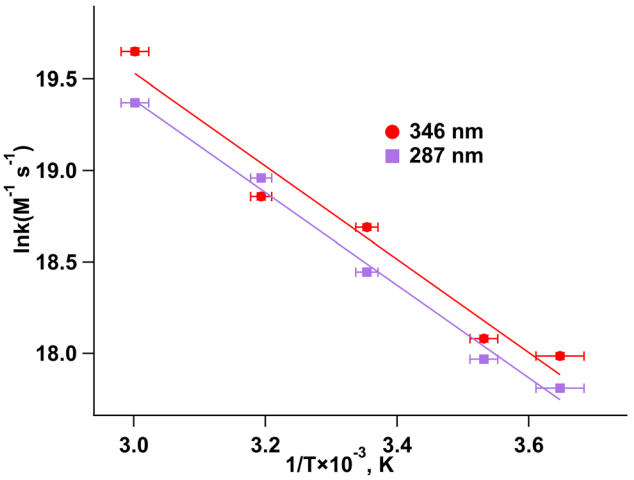

Fig. 3 The natural logarithm of the second-order rate constants measured at 346 nm and 287 nm for the reaction of Mn(II) with H atoms is plotted against the inverse temperature for $MnSO_4$ solutions at pH 3, over a temperature range from 1 °C to 60 °C. Arrhenius plot fit results are shown by the solid line ($\ln k_{0(346nm)} = -2549/T + 27.2$; $\ln k_{0(287nm)} = -2532/T + 27.0$).

temperature dependence of the second-order rate constants for the reaction of Mn(II) with H atoms across all measured solutions.

In all cases, the reaction rate increases with temperature. The Arrhenius plot shows the fitted second-order rate constants, corrected for ionic strength (k_0). The activation energy and pre-exponential factor were determined to be 21.2 ± 2 kJ mol^{-1} and (6.4 ± 4) × 10^{11} M^{-1} s^{-1} at 346 nm and 21.1 ± 2 kJ mol^{-1} and (5.3 ± 4) × 10^{11} M^{-1} s^{-1} at 287 nm, respectively (Table 2). The similar rate constants and Arrhenius parameters observed for these transients, which are formed from the reaction of Mn(II) with hydrogen atoms, suggest that they likely represent the same species. Dainton *et al.* measured the Arrhenius parameters for this reaction at 290 nm over the low-temperatures range from −83 °C to 7 °C. They reported an activation energy of 20 ± 2 kJ mol^{-1} and a pre-exponential factor of (1.8 ± 0.4) × 10^{12} s^{-1}. These values are similar to those obtained in our study. Comparable Arrhenius parameters were obtained for the reaction of Mn^{2+} with e_{aq}^- in the paper by Kanjana *et al.*,[8] as listed in Table 2.

Reactions of manganese ions with hydroxyl radicals

The reaction between Mn(II) species and •OH (eqn (11)) was also studied at pH 5 and 3. In N_2O-saturated acidic solutions, e_{aq}^- (eqn (12)) and H (eqn (13)) are rapidly converted into •OH, enhancing the yield of oxidizing species.[22]

$$Mn^{2+} + {}^{\bullet}OH \rightarrow Mn^{3+} + OH^- \quad (11)$$

$$e_{aq}^- + N_2O + H_2O \rightarrow {}^{\bullet}OH + OH^- + N_2, \quad k = 9.1 \times 10^9\ M^{-1}\ s^{-1} \text{ at } 25\ ^\circ C \quad (12)$$

$$H + N_2O \rightarrow {}^{\bullet}OH + N_2, \quad k = 2 \times 10^6\ M^{-1}\ s^{-1} \text{ at } 25\ ^\circ C \quad (13)$$

Fig. 4A shows transient absorption spectra observed for the reaction of Mn^{2+} with •OH at pH 3 and 5 at room temperature. It is notable that a broad peak forms at 250–310 nm, with an additional peak at 360 nm whose optical density increases at lower pH. Additionally, a weak peak can be observed at λ_{max} = 470 nm. Fig. 4B shows the kinetic traces at 285 nm, 346 nm, and 480 nm for Mn(II) solutions at pH 5 and pH 3. At the lower pH (pH 3), the formation and decay of the signal at 285 nm occur more rapidly, and the absorbance peak at 346 nm is noticeably more intense compared to pH 5. In contrast, there is no noticeable effect of pH on the peak at 480 nm.

The Mn^{3+} ion in aqueous solution is a strong Brønsted acid and can form two monomeric hydrolysis species of Mn^{3+} at very low pH and high ionic strength (eqn (14) and (15)):[23]

$$Mn^{3+} + H_2O \rightleftharpoons Mn(OH)^{2+} + H^+ \quad (14)$$

$$Mn^{3+} + 2H_2O \rightleftharpoons Mn(OH)^{2+} + 2H^+ \quad (15)$$

In the study by Davies,[23] both chemical and electrolytic methods were used to oxidize Mn(II) to Mn(III) at high concentrations. They reported that the spectra of Mn^{3+} and $MnOH^{2+}$ are similar, both showing an absorption maximum at 470 nm, attributed to a $^5T_{2g} \rightarrow {}^5E_g$ transition. $MnOH^{2+}$ has a higher extinction coefficient in the visible region compared to Mn^{3+}, while the Mn^{3+} peak is broader.

In the UV region, absorption maxima appear between 210–220 nm, likely due to electron transfer from ligand to metal involving σ-bonding.

The transient absorption spectra we observed are more consistent with those reported for Mn^{3+}, and at pH 3, there may be some contribution from $MnOH^{2+}$. However, it is important to note that the data reported by Davies[23] were obtained under high ionic strength conditions, which may influence the spectral features.

Henglein *et al.*[13] proposed that, during the oxidation of Mn(II) by •OH, Mn(III) is formed through intermediate species such as $MnOH^{2+}$ or $Mn(OH)_2^+$, with the specific pathway

Table 2 Arrhenius parameters for the reactions of Mn^{2+} with water radiolysis species

Reaction	λ, nm	E_a, kJ mol^{-1}	A, M^{-1} s^{-1}
$Mn^{2+} + e_{aq}^- \rightarrow Mn^+$	720	27.5[8]	3.8 × 10^{128}
$Mn^{2+} + H \rightarrow Mn^+$	290	21.1 ± 2; 20 ± 2 (0.01 M ionic strength)[11]	(5.3 ± 4) × 10^{11}; (1.8 ± 0.4) × 10^{12} (0.01 M ionic strength)[11]
	346	21.2 ± 2	(6.4 ± 4) × 10^{11}
$Mn^{2+} + {}^{\bullet}OH \rightarrow Mn^{3+} + OH^-$	285	27.2 ± 1	(6.1 ± 4) × 10^{11}
	480	23.5 ± 1	(1.6 ± 1) × 10^{11}
$Mn^{2+} + O_2{}^{\bullet-} \rightarrow [Mn{-}O_2]^+$	278	33.8 ± 2	(3.6 ± 2) × 10^{13}
	425	41.8 ± 2	(2.2 ± 3) × 10^{14}

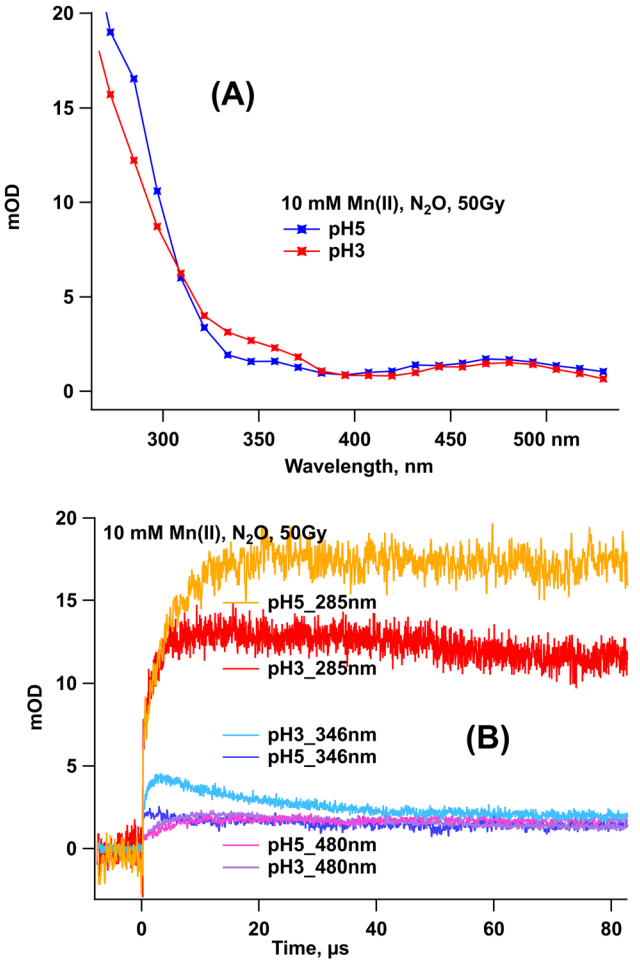

Fig. 4 Transient absorption spectra (A) and the kinetics at various wavelengths (B) observed 50 μs after 15-ns pulse radiolysis (50 Gy) in N_2O-saturated $MnSO_4$ solutions at pH 5 and 3 at room temperature.

depending on pH and a reported pK_a of 5. However, their paper only shows the final spectra after gamma irradiation of Mn(II) solutions at different pHs, plus a single spectrum recorded on the second timescale that does not display a peak at 470 nm.

Although, similar transient spectra showing a peak at 470 nm were reported by Pick-Kaplan and Rabani for Mn(II) in N_2O-saturated solutions at pH 6.7.[10] In their study, they suggested that Mn^{3+} is formed in the form of $MnOH^{2+}$.

The calculated rate constant for the formation of the transient species at room temperature at 285 nm was 1.0×10^7 M^{-1} s^{-1} at pH 5, and for the transient at 480 nm, it was 1.3×10^7 M^{-1} s^{-1}.

Previously, rate constants at about 260 nm were reported as 2.6×10^7 M^{-1} s^{-1} at pH 9[13] and 3.4×10^7 M^{-1} s^{-1} at pH 7,[10] and 2.0×10^7 M^{-1} s^{-1} at pH 0–6[12] at 25 °C; however, the corresponding transient species in other spectral regions were not identified.

We found that in acidic solutions at pH 3, the rate constant of the transient formed at 285 nm was two times higher (2.5×10^7 M^{-1} s^{-1}), and the decay kinetics were faster compared to pH 5, while the rate for the transition at 480 nm remained unchanged. Fig. S4 (SI) presents the obtained pseudo-first-order rate constants (k') were plotted against $MnSO_4$ concentration for the formation kinetics at 285 nm at pH 3 and 5 at room temperature. Nevertheless, in acidic solutions, the formation of a transient at 346 nm was also observed, with a rate constant of 6.2×10^7 M^{-1} s^{-1} at 25 °C. Under these acidic conditions, the reaction (eqn (14)) is expected to predominantly form the $Mn(OH)^{2+}$ species, as it releases fewer protons than in (eqn (15)). This species exhibits transient absorption bands in the 250–300 nm and 350 nm regions.

The reaction rate between Mn(II) and $^{\bullet}OH$ at pH 5 was measured at 285 nm and 480 nm at temperatures from 1 °C to 60 °C. As shown in Fig. S5, the Arrhenius plot is linear, indicating a consistent temperature dependence.

The calculated pre-exponential factor is $(6.1 \pm 4) \times 10^{11}$ M^{-1} s^{-1}, and the activation energy is 27.2 ± 1 kJ mol^{-1}. Slightly lower values were measured at 480 nm, as shown in Table 2.

These results, along with the fact that the kinetics of the transient formed at 480 nm did not change between pH 3 and 5, suggest the formation of the same intermediate under both conditions. The intermediate could be a Mn(III) species, which may form through a mechanism that does not depend on proton concentration and remains stable across this pH range.

At higher temperatures, we observed that Mn(II) solutions turned brown after irradiation. This color change, noticeable while recording transient absorption spectra, indicates the formation of manganese oxides.

Mn^{3+} is unstable in solution and readily undergoes disproportionation into Mn^{2+} and Mn(IV) oxide (eqn (16)).[23]

$$2Mn^{3+}_{(aq)} + 2H_2O \rightleftharpoons MnO_{2(s)} + Mn^{2+}_{(aq)} + 4H^+ \quad (16)$$

As shown in Fig. 5, irradiating 100 mM Mn(II) solutions under both N_2O-saturated and Ar-saturated conditions produced a broad absorption peak between 300–400 nm. The intensity was significantly stronger in the N_2O-saturated solution, where the highest concentration of $^{\bullet}OH$ is generated. These results confirm that electron pulse irradiation induces the formation of colloidal manganese oxides in Mn(II) solutions, and the rate of oxide formation increases with temperature. Previous studies support these findings. Pick-Kaplan and Rabani,[10] Baral *et al.*,[13] and later Yadav *et al.*,[25] reported the formation of manganese oxide colloids following the oxidation of Mn(II). Henglein demonstrated that manganese oxide colloids form within the pH range of 3.5 to 9[13] and proposed that the final oxide forms from $MnOH^{2+}$ or $Mn(OH)_2^+$ through two possible pathways: either *via* condensation to form Mn(III) oxide, or *via* condensation followed by disproportionation, leading to the formation of Mn(IV) oxides.

Thus, irradiation of Mn(II) solutions promotes temperature-dependent formation of manganese oxide colloids, especially under N_2O-saturated conditions, through intermediate species to yield Mn(IV) oxides.

Reactions of manganese ions with oxygen species

Upon radiolysis of water, the e_{aq}^- rapidly reacts with dissolved molecular oxygen to form $O_2^{\bullet-}$, a key intermediate in oxidative aqueous chemistry:[26]

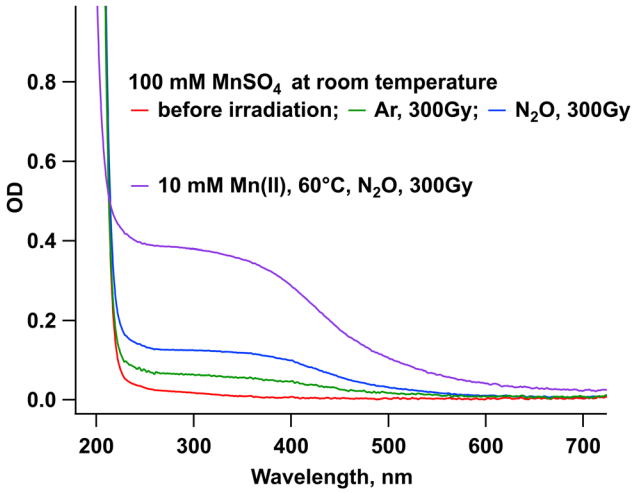

Fig. 5 Absorption spectra of products observed after pulse radiolysis in Ar- and N_2O-saturated solutions with 100 mM $MnSO_4$ at pH 5 at room temperature, as well as in 10 mM $MnSO_4$ solutions at 60 °C.

$$e_{aq}^- + O_2 \rightarrow O_2^{\bullet -}, \quad k = 1.8 \times 10^{10}\ M^{-1}\ s^{-1} \text{ at } 25\ ^\circ C \qquad (17)$$

The subsequent the reaction between Mn^{2+} and $O_2^{\bullet -}$ was studied in O_2-saturated solutions containing 0.1–1 mM $MnSO_4$, with the addition of methanol or tert-butanol, at pH about 5, at room temperature. Fig. 6 shows a representative set of kinetic traces collected after a 15 ns at 278 nm and 425 nm, capturing the maximum change in optical absorbance associated with the formation of the $[Mn–O_2]^+$ adduct (eqn (18)).

$$Mn^{2+} + O_2^{\bullet -} \rightarrow [Mn–O_2]^+ \qquad (18)$$

The maximum absorbance of the adduct occurs between 5 and 30 μs, depending on the Mn^{2+} concentration, with the lifetime decreasing as concentration of Mn^{2+} increases.

Similar spectral features were observed in the presence of methanol or tert-butanol, which effectively scavenge $^\bullet$OH and H atoms (eqn (8) and (9)). In the absence of these scavengers, the same signal was present, but its intensity was reduced. This decrease is attributed to a competitive side reaction, where $O_2^{\bullet -}$ reacts with $^\bullet$OH at a high rate (eqn (19)),[27] reducing the availability of $O_2^{\bullet -}$ for adduct formation with Mn^{2+}.[12]

$$^\bullet OH + O_2^{\bullet -} \rightarrow O_2 + OH^-, \quad k = 1 \times 10^{10}\ M^{-1}\ s^{-1} \text{ at } 25\ ^\circ C \qquad (19)$$

The rate constant, corrected for ionic strength, for the reaction at 26 °C was determined to be $4.3 \times 10^7\ M^{-1}\ s^{-1}$ at 278 nm and $3.5 \times 10^7\ M^{-1}\ s^{-1}$ at 425 nm. However, the decay kinetics at these wavelengths differ, which may be explained by the formation of different transient species. This value is reasonably close to the previously reported rate of $5 \times 10^7\ M^{-1}\ s^{-1}$ observed in similar experiments using formate as the $^\bullet$OH scavenger at 25 °C.[14] Cabelli and Bielski[14,28] investigated reaction eqn (18) in the presence of various anions, including formate, sulfate, phosphate, and pyrophosphate. In this reaction, they observed the formation of Mn^{3+} at neutral pH when phosphate or pyrophosphate was present. In these papers, the authors recorded transient spectra only up to 350 nm, so there is no data available at 425 nm.

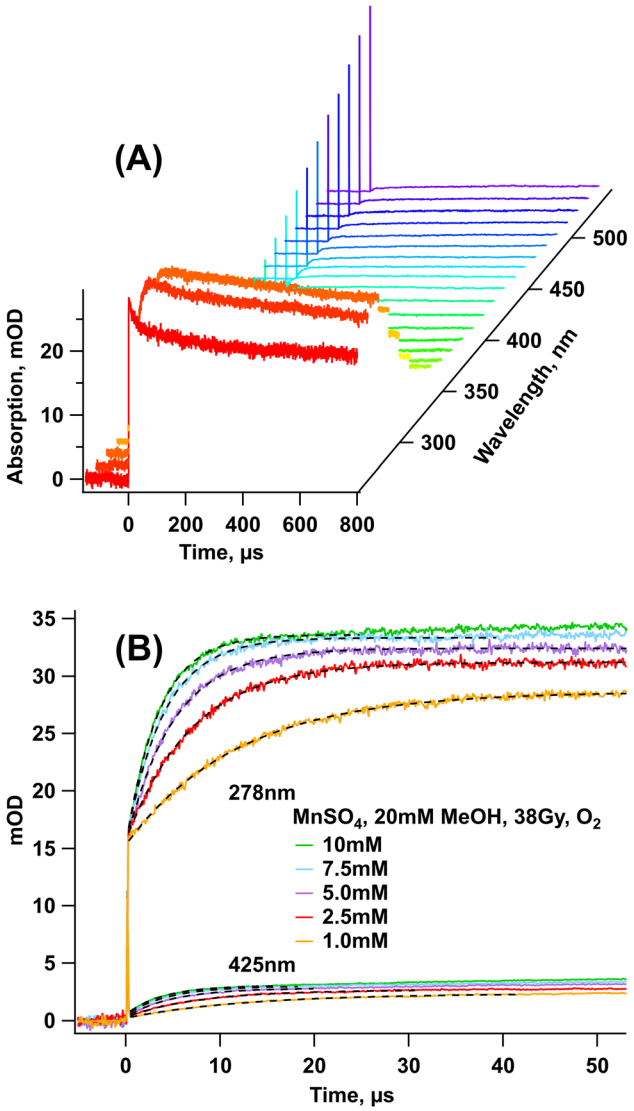

Fig. 6 Transient absorption spectra (A) and the kinetics at 278 and 425 nm (B) observed after 15-ns pulse radiolysis (38 Gy) in O_2-saturated $MnSO_4$ solutions with 20 mM MeOH at pH 5 at room temperature.

However, Pick-Kaplan and Rabani reported similar transient absorption spectra arising from Mn(II) under radiolysis conditions in both N_2O- and O_2-saturated aqueous solutions at pH 6.7.[10] In contrast, our experiments in N_2O-saturated solutions show a different transient absorption spectrum, with a peak around 480 nm. In the paper,[10] the authors studied how rate constants changed when using formate and perchlorate salts at different concentrations. They explained these changes as being caused by both ionic strength and the ability of the salts to form complexes. These observations indicate that reaction pathways and intermediates may differ depending on conditions used, potentially involving complexation and ionic strength effects.

We investigated the temperature dependence of this reaction by conducting experiments from 1 °C to 65 °C. The resulting Arrhenius plot (Fig. S6) shows a linear relationship, indicating that the reaction follows Arrhenius behavior.

From the slope and intercept of the plot, we determined an activation energy of 33.8 ± 2 kJ mol^{-1} for the transient at 278 nm and 41.8 ± 2 kJ mol^{-1} at 425 nm, with pre-exponential factors of (3.6 ± 2) × 10^{13} M^{-1} s^{-1} and (2.2 ± 3) × 10^{14} M^{-1} s^{-1}, respectively. A summary of the ionic strength–corrected rate constants and Arrhenius parameters is provided in Tables 1 and 2.

The higher activation energy and larger entropy component observed for the reaction between Mn^{2+} and $O_2^{\bullet-}$ compared to its reactions with •OH, H, or e_{aq}^-, likely reflect the lower reactivity and greater selectivity of $O_2^{\bullet-}$.

Conclusions

We investigated the reduction of Mn^{2+} by e_{aq}^- in Ar-saturated aqueous solutions across pH 1.6–6, observing the formation of Mn(I) transient species with characteristic UV absorption at 290 and 360 nm. Additional experiments demonstrated that Mn(I) can also form through reduction by hydrogen atoms, with a rate constant of 1.0 × 10^8 M^{-1} s^{-1} at 25 °C. The reaction between Mn(II) and •OH at pH 3 and 5 produces transient species with characteristic peaks at 290, 350, and 480 nm, and a rate constant of 1.0 × 10^7 M^{-1} s^{-1} was determined for the 290 nm species at pH 5 at 25 °C. Temperature-dependent studies of the reactions of Mn(II) with H atom, and •OH revealed that they follow Arrhenius behavior, with activation energies ranging from 21 to 27 kJ mol^{-1}.

Mn(II) was also found to react with $O_2^{\bullet-}$, forming transient absorption signals at 278 and 425 nm, consistent with the formation of a $[Mn–O_2]^+$ adduct. A rate constant of 4.3 × 10^7 M^{-1} s^{-1} was determined for the 290 nm species at 25 °C. This reaction showed a consistent thermal activation process, following a linear Arrhenius trend up to 65 °C. Compared to its reactions with hydroxyl radicals, hydrogen atoms, or hydrated electrons, the reaction of Mn(II) with the superoxide exhibited a higher activation energy, suggesting lower reactivity but greater selectivity of the $O_2^{\bullet-}$.

These kinetic and mechanistic parameters are critical for modelling redox transformations in nuclear reactor chemistry, particularly under radiolytic conditions. They also enhance our understanding of manganese speciation and reactivity in environmental systems influenced by radiation or redox-active species.

Author contributions

AL: experiment, data analysis, writing, supervision. IT, BS, ND: experiment, data analysis.

Conflicts of interest

There are no conflicts to declare.

Data availability

The data supporting the findings of this study are available within the article and its SI. Additional datasets generated and/or analyzed during the current study are available from the corresponding author on reasonable request.

Supplementary information available: Kinetic traces, spectral data, and analysis of hydrated electron decay, manganese(I) formation, and manganese(II) reactions with hydroxyl radical and superoxide. Data are presented for various pH values and temperatures, including Arrhenius plots, and tables of rate constants for water radiolysis species and their reactions with manganese(II). See DOI: https://doi.org/10.1039/d5cp02625c

Acknowledgements

The pulse radiolysis experiments at the Notre Dame Radiation Laboratory were supported by the U.S. Department of Energy, Office of Science, Office of Basic Energy Sciences under award number DE-FC02-04ER15533. This is document number NDRL-5476 from the Notre Dame Radiation Laboratory.

References

1 S. L. Suib, *Acc. Chem. Res.*, 2008, **41**, 479–487.
2 L. Tian, X. Zhai, X. Wang, J. Li and Z. Li, *J. Mater. Chem. A*, 2020, **8**, 14400–14414.
3 Y. Gorlin and T. F. Jaramillo, *J. Am. Chem. Soc.*, 2010, **132**, 13612–13614.
4 R. B. Jones, *Int. Mater. Rev.*, 2011, **56**, 167–206.
5 J. W. T. Spinks and R. J. Woods, *An introduction to radiation chemistry*, John Wiley and Sons Inc, 1990.
6 A. Lisouskaya, U. S. Markad, I. Carmichael and D. M. Bartels, *Phys. Chem. Chem. Phys.*, 2022, **24**, 19882–19889.
7 U. S. Markad, A. Lisouskaya and D. M. Bartels, *J. Phys. Chem. B*, 2023, **127**, 2784–2791.
8 K. Kanjana, B. Courtin, A. MacConnell and D. M. Bartels, *J. Phys. Chem. A*, 2015, **119**, 11094–11104.
9 J. H. Baxendale, E. M. Fielden and J. P. Keene, *Proc. R. Soc. London, Ser. A*, 1965, **286**, 320–336.
10 M. Pick-Kaplan and J. Rabani, *J. Phys. Chem.*, 1976, **80**, 1840–1843.
11 F. S. Dainton, N. A. Philipson and M. J. Pilling, *J. Chem. Soc., Faraday Trans. 1*, 1975, **71**, 2377–2383.
12 F. Jacobsen, J. Holcman and K. Sehested, *J. Phys. Chem. A*, 1997, **101**, 1324–1328.
13 S. Baral, C. Lume-Pereira, E. Janata and A. Henglein, *J. Phys. Chem.*, 1986, **90**, 6025–6028.
14 D. Cabelli and B. Bielski, *J. Phys. Chem.*, 1984, **88**, 6291–6294.
15 A. Elliot and D. Bartels, The reaction set, rate constants and *G*-values for the simulation of the radiolysis of light water over the range 20 deg to 350 deg C based on information available in 2008, Atomic Energy of Canada Limited, Mississauga, Ontario (Canada), 2009.
16 A. Lisovskaya, K. Kanjana and D. M. Bartels, *Phys. Chem. Chem. Phys.*, 2020, **22**, 19046–19058.

17 G. V. Buxton and C. R. Stuart, *J. Chem. Soc., Faraday Trans.*, 1995, **91**, 279.
18 P. L. Houston, *Chemical kinetics and reaction dynamics*, Courier Corporation, 2006.
19 J. Heller, E. M. Cunningham, C. van der Linde, M. Ončák and M. K. Beyer, *J. Phys. Chem. Lett.*, 2022, **13**, 3269–3275.
20 P.-Y. Jiang, Y. Katsumura, R. Nagaishi, M. Domae, K. Ishikawa, K. Ishigure and Y. Yoshida, *J. Chem. Soc., Faraday Trans.*, 1992, **88**, 1653–1658.
21 G. G. Jayson, B. J. Parsons and A. J. Swallow, *J. Chem. Soc., Faraday Trans. 1*, 1973, **69**, 1597–1607.
22 G. V. Buxton, C. L. Greenstock, W. P. Helman and A. B. Ross, *J. Phys. Chem. Ref. Data*, 1988, **17**, 513–886.
23 G. Davies, *Coord. Chem. Rev.*, 1969, **4**, 199–224.
24 S. Baral, C. Lume-Pereira, E. Janata and A. Henglein, *J. Phys. Chem.*, 1985, **89**, 5779–5783.
25 P. Yadav, R. T. Olsson and M. Jonsson, *Radiat. Phys. Chem.*, 2009, **78**, 939–944.
26 A. J. Elliot, D. R. McCracken, G. V. Buxton and N. D. Wood, *J. Chem. Soc., Faraday Trans.*, 1990, **86**, 1539–1547.
27 A. J. Elliot and G. V. Buxton, *J. Chem. Soc., Faraday Trans.*, 1992, **88**, 2465–2470.
28 D. Cabelli and B. Bielski, *J. Phys. Chem.*, 1984, **88**, 3111–3115.